S&G 15 (2020), pp. 235-249

S&G JOURNAL
ISSN: 1980-5160

STUDY OF LIFE CYCLE OF THE SUBTROPICAL CYCLONE ARANI IN THE SOUTH ATLANTIC IN MARCH 2011 THROUGH THE ERA-INTERIM AND CFSR REANALYSES

Ana Cristina Pinto de Almeida Palmeira
anactn@gmail.com
Federal University of Rio de Janeiro - UFRJ, Rio de Janeiro, Brazil.

Rodrigo de Souza Barreto Mathias
rodrigowind.meteoro@gmail.com
Brazilian Navy, Rio de Janeiro, Brazil.

ABSTRACT

Cyclone Arani occurred in March 2011 in the South Atlantic Ocean and was initially classified as a subtropical depression. When it reached winds above 34 knots, it passed to the subtropical storm category, and was named by the Brazilian Navy as Arani, which means furious weather in Tupi Guarani. This paper aimed to analyze the cyclone Arani through the Cyclone Phase Space, built with data from the European Centre for Medium-Range Weather Forecasts (ECMWF) ERA-interim reanalysis, with 0.7º spatial resolution, and also using synoptic fields and profiles with data from the Climate Forecast System Reanalysis (CFSR), with 0.5º resolution. Through the phase diagrams it was possible to identify the subtropical structure of cyclone Arani and the indication of an extratropical phase transition at the end of its life cycle. The results also indicated that the quality of the phase diagrams for cyclones with weak warm cores and small dimensions depends on adequate atmospheric models and therefore, the values obtained should be carefully analyzed when using global models. In this case, the qualitative study of the diagrams proved to be more useful than the purely quantitative analysis. Although disagrees with the information of an extratropical phase transition at the end of the cyclone Arani's life cycle, contained in the phase diagrams used in the study, the analysis of the fields and synoptic profiles contributed to the understanding of the cyclone's development and to the interpretation of the diagrams.

Keywords: Arani Subtropical Cyclone; South Atlantic; Cyclone Phase Space

PROPPI / DOT
DOI: 10.20985/1980-5160.2020.v15n3.1663

S&G Journal
Volume 15, Number 3, 2020, pp. 235-249
DOI: 10.20985/1980-5160.2020.v15n3.1663

1. INTRODUCTION

Cyclones spend much of their life cycle over the oceans. The operational weather forecast centers, focused on maritime areas, should pay special attention to these phenomena. The damages range from the destruction of the shores due to surges, to the non-functioning of the ports and the impossibility of maritime traffic due to adverse weather and sea conditions, not to mention the possible irreparable loss of human lives.

For approximately a century, the different types of cyclones were studied separately and were classified according to their area of formation into two basic types: extratropical and tropical (Hart; Evans, 2001). However, the advance in data collection, the increase in the quantity and quality of atmospheric observations over ocean areas through satellites and the development of numerical modeling tools have allowed to observe that extratropical cyclones can have tropical aspects, and vice versa. Thus, the same cyclone can present different phases during its life cycle, with different structural and thermal characteristics.

After the atypical occurrence of cyclone Catarina in 2004, meteorological institutions, universities and weather forecasting centers in Brazil have been emphasizing the study and prediction of the impact of cyclones on coastal areas. The International Meeting of South Atlantic Cyclones, which took place in May 2008, was another step of the Brazilian scientific community in search of improving knowledge about cyclones. The event, which was held in the city of Rio de Janeiro, brought together researchers and weather forecasters from various countries, in addition to bringing new knowledge and forecasting tools for tropical, extratropical, subtropical and hybrid cyclones. Among these new tools, the concept of Cyclone Phase Space was presented in detail.

Hart (2003) proposed the Cyclone Phase Space (CPS), which allows to evaluate the thermal structure of cyclones based on objective indicators. These indicators are the parameters B (cyclone thermal symmetry), $-V_T^L$ (thermal wind at low levels of the atmosphere) and $-V_T^U$ (thermal wind at high levels of the atmosphere), which define the phase of the cyclone. When the cyclone goes from one phase to another, it is said that there has been a phase transition of the cyclone that can be complete or partial, depending on whether or not the cyclone takes on the tropical or extratropical characteristics after the transition.

The phase that the cyclone assumes during its life cycle implies variations in its intensity, size, prediction uncertainty, and consequently the threat it poses to the coastal population and to navigators. Therefore, in order to increase the predictability of the trajectory and intensity of cyclones, the knowledge of the different thermal characteristics that they can present constitutes an important prognostic tool.

This article presents the thermal characteristics of the cyclone Arani, matching its structural changes of intensity with its evolution in cyclone phase diagrams.

2. MATERIAL AND METHODS

The information used was from the Climate Forecast System Reanalysis (CFSR), images from the GOES-12 satellite, synoptic charts prepared by the Marine Meteorological Service (MMS), operated by the Brazilian Navy Hydrographic Center (*Centro de Hidrografia da Marinha* - CHM), the Center for Weather Forecasting and Climate Studies (*Centro de Previsão do Tempo e Estudos Climáticos* - CPTEC/INPE), data estimated by satellite sensors (ASCAT and TRMM), and cyclone phase diagrams with ERA-Interim reanalysis data generated by Florida State University (FSU), during the formation and development period of the Arani Cyclone, March 13-19, 2011.

Climate Forecast System Reanalysis (CFSR)

The CFSR is a high-resolution information database. The second version was implemented in 2010, covering the period from January 1979 to the present day (Saha *et al*., 2010). The data are available in 64 pressure levels, ranging from surface to 0.26 hPa, with horizontal spacing of 0.5° and frequency of 1 hour.

The reanalysis data were generated through the Global Forecast System (GFS) model and, as an oceanic model, the fourth version of the Modular Ocean Model (MOM4), therefore with air-sea coupling.

In this work the information is available in four synoptic times (00Z, 06Z, 12Z and 18Z) with 28 pressure levels, from the surface to 100 hPa (surface, 1000, 975, 950, 925, 900, 875, 850, 825, 800, 775, 750, 700, 650, 600, 550, 500, 450, 400, 350, 300, 250, 225, 200, 175, 150, 125 e 100 hPa), in addition to the wind data at 10 meters. The fields and profiles of the reanalysis data were obtained through the Grid Analysis and Display System (GrADS) (Doty; Kinter, 1995), in version 2.0.a9 for Linux.

For the synoptic analysis of the cyclone, the fields of geopotential in 500 hPa and the jet in 250 hPa were used in superposition to the pressure at the surface, in order to verify possible contributions of the circulation in medium and high levels of the atmosphere over the cyclone; pressure at the surface with the thickness of the layer between

900 hPa and 600 hPa, to identify the thermal nature of the air masses that interacted with the cyclone; and wind at 10 meters to identify the intensity variations of the cyclone at the surface during its evolution. The vertical cross sections were made over the latitude where the minimum pressure of the cyclone was at surface, at each moment, within the domain of longitudes which it developed over the South Atlantic Ocean (050W-010W). The geopotential disturbance profiles were obtained within a radius of 500 km around the position of the cyclone center at surface, according to Hart's methodology (2003).

Satellite images and estimates

The images of the GOES-12 satellite, on the infrared channel, were obtained upon request from the Environmental Satellite Division (DSA) of the National Institute for Space Research (INPE).

Other satellite derived products were used, such as the Sea Surface Temperature (SST) and winds over ocean surfaces estimation. The SST data were obtained through the TRMM Microwave Imager (TMI) microwave sensor, aboard the Tropical Rainfall Measuring Mission (TRMM) satellite and are available on the Remote Sensing Systems (RSS) web page (http://images.remss.com/tmi/tmi_data_daily.html). Wind data at 10 meters were obtained from the ASCAT marine wind scatometer on board the EUMETSAT METOP satellite (https://manati.star.nesdis.noaa.gov/datasets/ASCATData.php).

Synoptic charts

Synoptic charts (subjective analysis) made by SMM, operated by CHM, (https://www.marinha.mil.br/chm/dados-do-smm-cartas-sinoticas/cartas-sinoticas), and CPTEC/INPE (http://img0.cptec.inpe.br/~rgptimg/Produtos-Pagina/Carta-Sinotica/Analise/Superficie/) were used.

Cyclone Phase Space

It is a three-dimensional space defined by three parameters that characterize the cyclone: "B", referring to the cyclone's thermal symmetry, indicating whether the cyclone is frontal or non-frontal, and "-V_T^L" and "-V_T^U", referring to its thermal structure and corresponding to the thermal wind between 900 hPa and 600 hPa, and between 600 hPa and 300 hPa, respectively. These last parameters indicate the thermal nature of the cyclone, that is, whether they have a cold core or a warm core in the respective atmospheric layers considered. The three parameters define the x, y and z axes of this phase space.

The analyzed phase diagrams were prepared by FSU with the reanalysis data from the ERA-Interim project of the European Centre for Medium-Range Weather Forecasts (ECMWF), with horizontal resolution of 0.7.

Parameter B: cyclone thermal symmetry

Considering that the atmospheric layer has a certain average temperature, it is concluded that the thickness of the layer between two vertical levels of pressure is directly proportional to this temperature. Therefore, where there is cold advection in a certain layer of the atmosphere there is a tendency to reduce the thickness of this layer, while where there is warm advection, the fluid tends to expand and the layer has its thickness increased. In this way, an isobaric surface that passes over an extratropical cyclone will present asymmetric levels of geopotential height. Tropical cyclones that form in areas of great thermal homogeneity perform little or no temperature advection, resulting in great thermal symmetry and, consequently, a strong symmetry in the geopotential height field.

The parameter B was proposed to quantify the degree of symmetry of the cyclone and, therefore, its frontal or non-frontal nature. It measures the average layer thickness gradient between 900 hPa and 600 hPa (which is directly proportional to the average temperature gradient of the layer), perpendicular to the cyclone movement, within a radius of 500 km from the center of the cyclone in surface (Equation 2.1).

$$B = h\left(\overline{Z_{600\,hPa} - Z_{900\,hPa}}\Big|_D - \overline{Z_{600\,hPa} - Z_{900\,hPa}}\Big|_E\right) \quad 2.1$$

In which

h= +1 for HN and h= -1 for HS;

Z_{600hPa} is the geopotential height at the level of 600 hPa;

Z_{900hPa} is the geopotential height at the level of 900 hPa;

and the indices "D" and "E" correspond to the right and left sides of the cyclone, respectively, and their reference is the dividing line established by their displacement vector.

A mature tropical cyclone has a B value of approximately zero, while an extratropical cyclone in development has a large positive B value. The final stages of an extratropical cyclone also have small values of B, since after the occlusion occurs the elevation of its warm sector and mixing of the air masses, resulting in a center of homogeneous cold

S&G Journal
Volume 15, Number 3, 2020, pp. 235-249
DOI: 10.20985/1980-5160.2020.v15n3.1663

low pressure. Hart (2003) established the criterion B = 10 meters to distinguish symmetrical from asymmetrical cyclones and this criterion will be used in this study.

Parameters $-V_T^L$ and $-V_T^U$: thermal wind and core thermodynamics

The thermal nature of the cyclone core, warm or cold, can be known through the analysis of the thermal wind across the entire vertical extent of the cyclone center. The vector relationship of the thermal wind is indicated in Equation 2.2:

$$\overrightarrow{V_T} = \frac{g}{f}\hat{k} \times \vec{\nabla} Z_T \qquad 2.2$$

where,

V_T is the thermal wind; g is the acceleration of gravity; f is the Coriolis parameter; and ∇Z_T is the horizontal gradient of the thickness of the atmospheric layer.

Considering that all cyclones can have both warm and cold cores simultaneously, depending on the atmospheric layer examined (Hirschberg; Fritsch, 1993), were created the $-V_T^L$ parameter, which analyzes a layer representative of the low levels of the troposphere (900 hPa to 600 hPa), and the $-V_T^U$ parameter, which analyzes a layer representative of the high levels of the troposphere (600 hPa to 300 hPa). The layer below 900 hPa is not included to prevent extrapolation below ground or within the atmospheric boundary layer, which is not always representative of the cyclone structure in the free atmosphere. The atmosphere above 300 hPa is excluded to prevent the influence of the stratospheric phase, which is often opposed to the tropospheric phase.

Positive values of $-V_T$ indicate a warm core layer, while negative values indicate a cold core layer. For a tropical warm core cyclone, $-V_T^L$ and $-V_T^U$ are necessarily positive and $-V_T^L$ has a higher magnitude. Conversely, for an extratropical cold core cyclone, $-V_T^L$ and $-V_T^U$ are necessarily negative and $-V_T^U$ has a greater magnitude. In hybrid cyclones, extratropical cyclones with warm seclusion or subtropical cyclones, $-V_T^L$ and $-V_T^U$ present opposite signs.

The warm and cold cores of a cyclone are related directly to its vertical structure of the geopotential height disturbance (amplitude). The presence of a cold core indicates a cyclone wave or structure with greater amplitude at the top of the layer than at the base, with the trough axis leaning westward. Inversely, the warm core presents a geopotential height disturbance that is greater at the base than at the top of the layer, with the trough axis approximately vertical (stacked).

It is worth noting that although Gozzo *et al.* (2014) used different thresholds both for parameter B and for thermal winds in their studies of subtropical cyclones over the South Atlantic, in this work, Hart's (2003) criterion was used exactly for the Arani life cycle analysis.

3. RESULTS AND DISCUSSION

Synoptic description, dynamics, and observational aspects

On March 14, 2011, areas of low pressure deepened near the coast of the Brazilian states of Rio de Janeiro and Espírito Santo and gave rise to a cyclone that developed over the South Atlantic Ocean. From the 15th, the cyclone was classified by the Brazilian Navy as subtropical storm "Arani", according to a list of names that is included in the Maritime Authority Standards for Maritime Meteorological Activities (NORMAM-19), and which was established to name tropical and subtropical cyclones that form over the Brazilian maritime area of responsibility, known as METAREA V.

According to the criteria established by Jarvinen *et al.* (1984), the subtropical cyclone Arani was classified as a subtropical depression from its origin (winds below 34 knots), near the coast, until its intensification and category elevation (Figures 1A and 1B). On the 15th, the cyclone was classified as a subtropical storm, as the winds exceeded 34 knots (Figures 1C and 1D).

Although the Atlantic Ocean is not officially monitored by the US Meteorological Service, Cyclone Arani has been classified by the National Hurricane Center (NHC) as the INVEST 90Q case. It is worth noting that an INVEST case means the existence of an area that deserves to be investigated due to its potential for tropical cyclone formation. From this classification, the NHC has made available outputs of the GFDL model (Figure 2 A-B), which is more suitable for the prognosis of tropical developments and is used for forecasting hurricanes over the North Atlantic Ocean. It was also indicated a minimum Pressure at Mean Sea Level (PMSL) of 994 hPa between the 14th and the 16th (not shown).

The MMS represented the cyclone in its synoptic charts as a subtropical storm, with a minimum pressure of 998 hPa, on the 15th at 1200Z. From the 17th, the MMS indicated the extratropical transition of the cyclone, evidenced by

S&G Journal
Volume 15, Number 3, 2020, pp. 235-249
DOI: 10.20985/1980-5160.2020.v15n3.1663

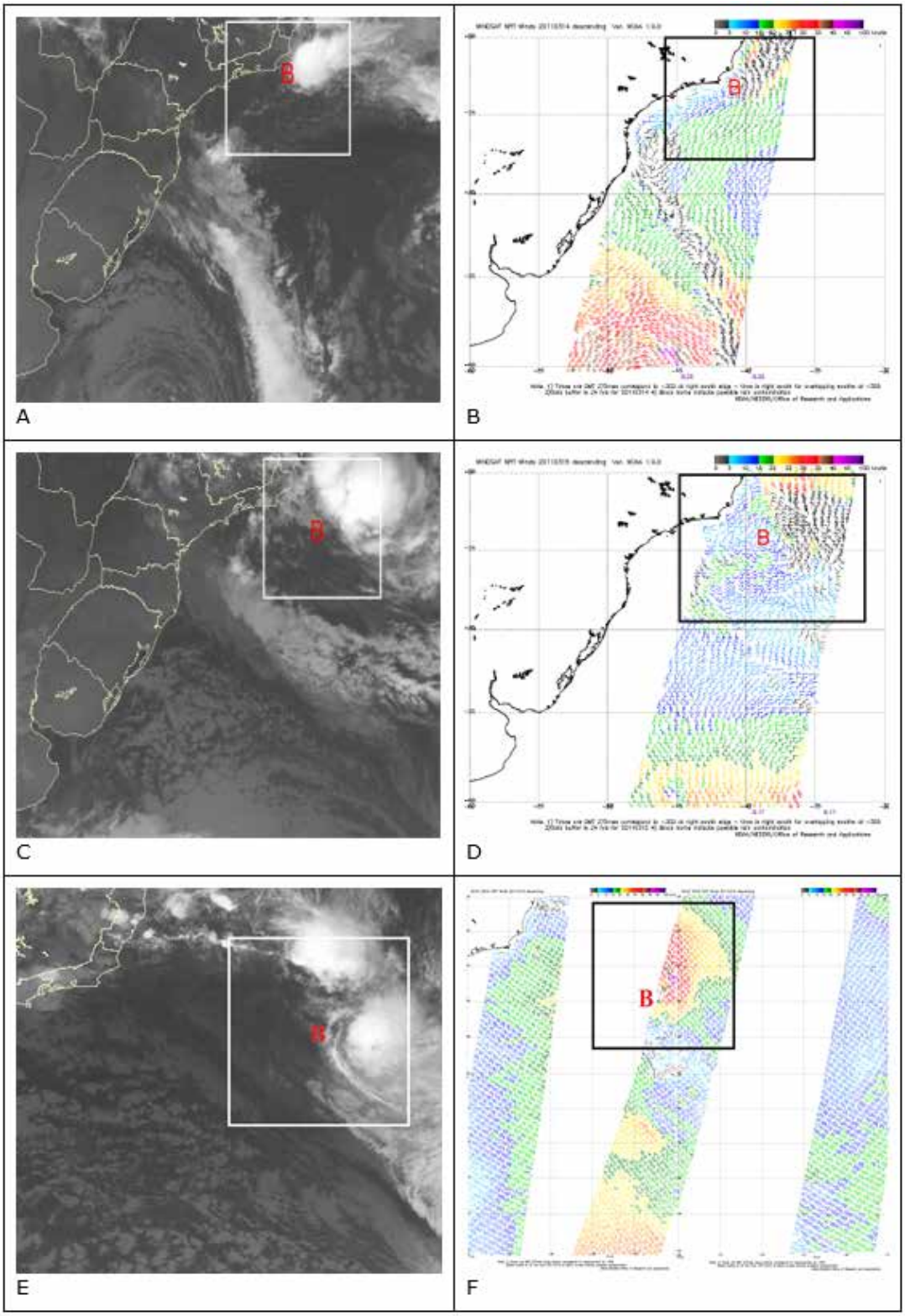

Figure 1. GOES-12 satellite images on the infrared channel. In prominence is the cyclone Arani (A) at 140600Z, (C) at 150600Z and (E) at 161200Z. Estimates of the surface wind speed through the ASCAT scatometer (B) at 140600Z, (D) at 150600Z and (E) at 161000Z. The letter B, in red, indicates the approximate position of the minimum pressure associated with the cyclone. The maximum winds observed in (B) do not exceed 30 knots; in (D) they are between 30 and 40 knots; and in (F) they are between 40 and 45 knots north and northeast of the center of the cyclone. [Source: NOAA].

S&G Journal
Volume 15, Number 3, 2020, pp. 235-249
DOI: 10.20985/1980-5160.2020.v15n3.1663

the presence of a cold front in its synoptic chart (Figure 2 C-D). The Weather Forecasting Group (WFG) of CPTEC/INPE has also indicated the phase transition of the cyclone from day 17, drawing a cold front on the 180000Z chart (Figure 3).

The high SSTs observed supported the development of intense convective activity and the deepening of the cyclone. The maximum temperatures estimated by satellite in the area of its development (Figure 4) were close to 30ºC, which is favorable to tropical cyclogenesis.

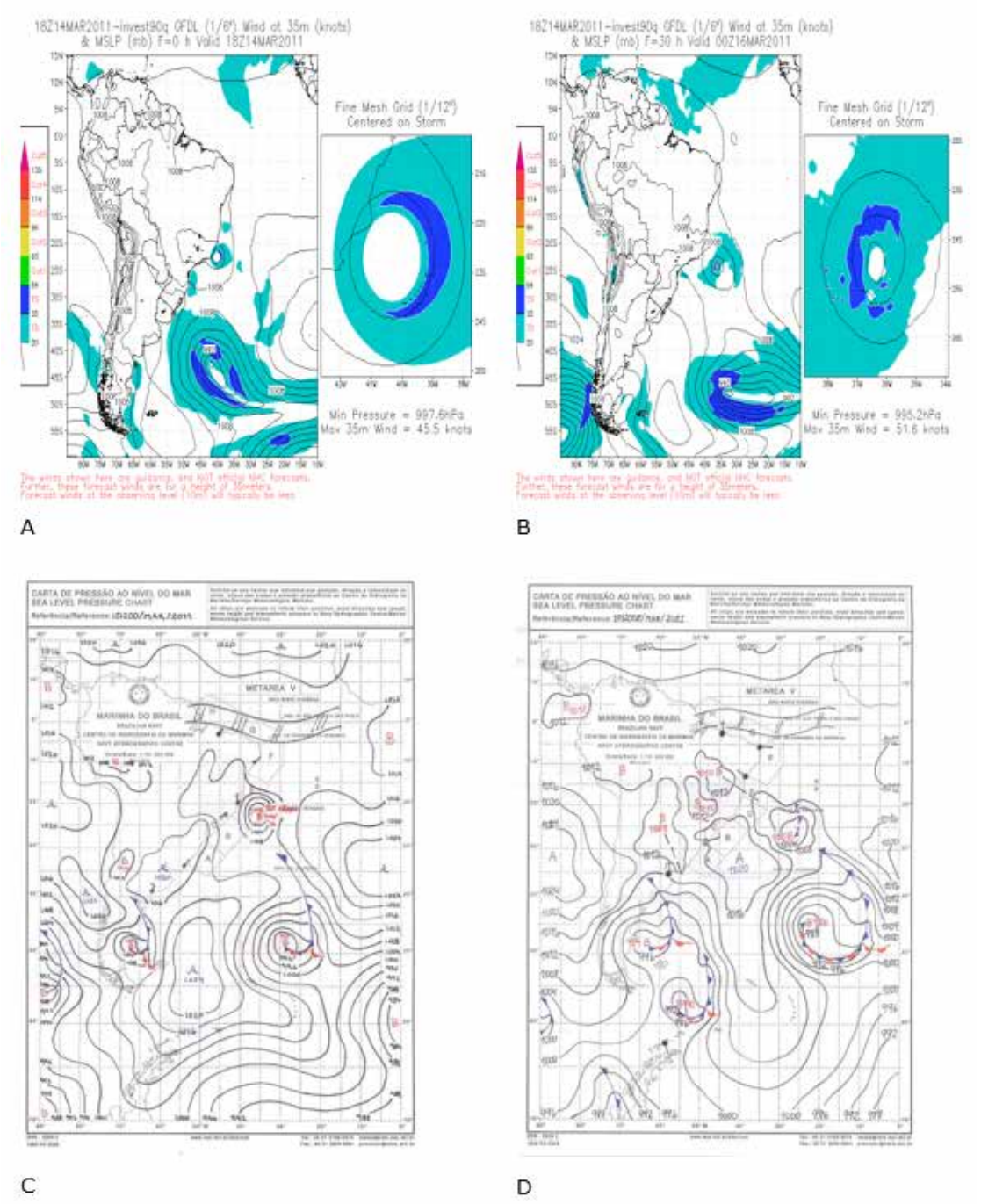

Figure 2. Pressure field at the surface and wind at 35 m from the GFDL model with grids of 1/3° and 1/6°, the last one centered on the cyclone. Analysis from March 14, 2011 at 18Z in (A) and forecast for March 16, 2011 at 00Z in (B) (Source: NHC). And synoptic charts of MMS/Brazilian Navy showing the Arani Subtropical Storm in 151200Z in (C) and the subsequent frontogenesis in 171200Z in (D). [Source: Centro de Hidrografia da Marinha/MB]

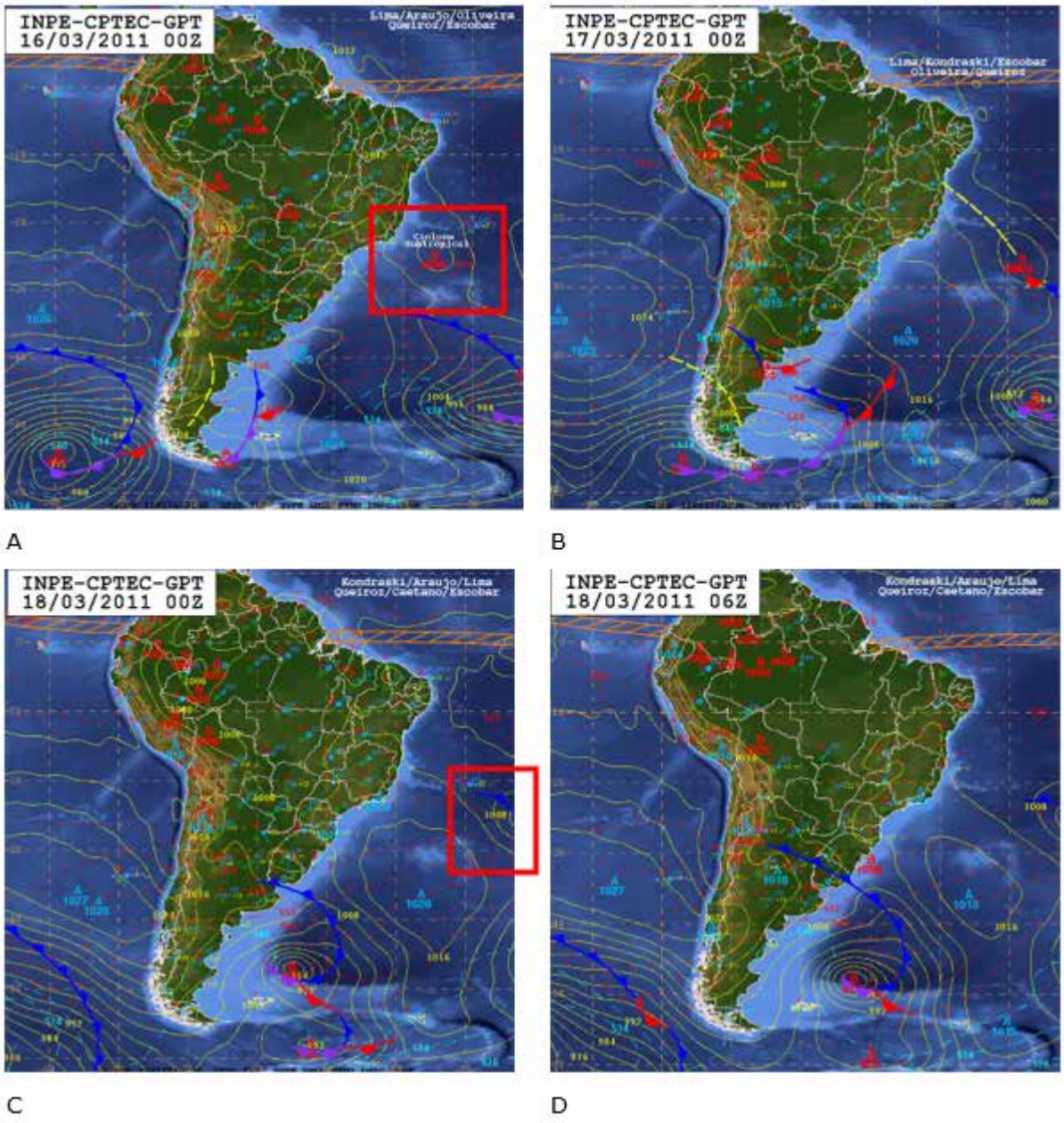

Figure 3. CPTEC/INPE synoptic charts. Highlighting the subtropical cyclone Arani, during the 16th and the 17th (A and B), and the subsequent appearance of a cold front in the cyclone (C and D). [Source: CPTEC/INPE]

By CFSR reanalysis, the cyclone had a minimum pressure value estimated at 1004 hPa (Figures 5A, 5D, and 5G). It was not associated with significant thermal gradients at low levels and developed in a warm and homogeneous air mass, without evident temperature contrasts in the layer between 900 hPa and 600 hPa (Figures 5C, 5F, and 5I), which can also be deduced by the absence of a jet at 250 hPa in the vicinity of the cyclone (Figures 5B, 5E, and 5H). A medium level trough was in phase with the cyclone in surface, denoting barotropic characteristic (Figures 5A, 5D, and 5G).

Unlike Cyclone Catarina (Gan, 2009), which occurred in March 2004, Cyclone Arani showed continuous movement east/southwest and its convective activity was not organized in the form of spiral bands, typical of tropical cyclones. The deeper convection remained slightly away from the center of the cyclone, in its eastern and northeastern sectors. The cloud band and the maximum winds observed away from the center of the cyclone are characteristics consistent with those predicted by Herbert; Poteat (1975) for subtropical cyclones.

S&G Journal
Volume 15, Number 3, 2020, pp. 235-249
DOI: 10.20985/1980-5160.2020.v15n3.1663

From the 16th, a cold front that moved further south, in a southwest-northeast direction, approached cyclone Arani. There was the coupling of the trough in 500 hPa associated to the cyclone Arani and the middle latitudes baroclinic trough that gave dynamic support to the frontal system (Figures 5A, 5D, and 5G).

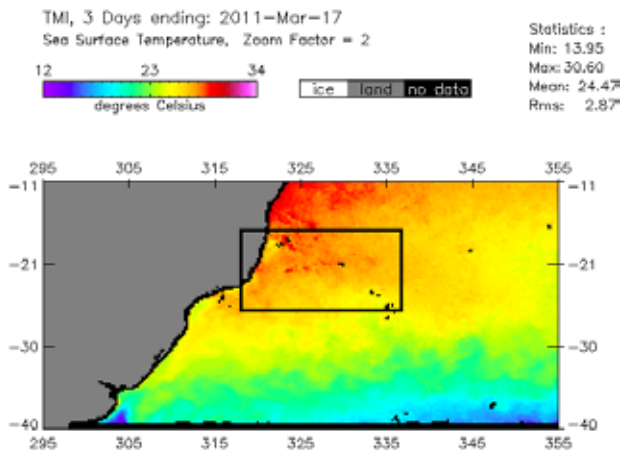

Figure 4. Estimate of average SST on March 15, 16 and 17 through the microwave sensor on board the TRMM satellite. [Source: Remote Sensing Systems (RSS)].

The CFSR reanalysis points out that the cyclone Arani had maximum sustained wind between 30 and 35 knots (Figure 6), which are underestimated values when faced with satellite estimates (Figure 1). This difference can be attributed to the underestimated representation, by CFSR, of cyclone pressures and their pressure gradient.

Analysis of the phase diagrams

The phase diagrams of the cyclone Arani can be seen in Figure 7, where A and B relate thermal symmetry (parameter B) and thermal wind (parameter $-V_T^L$) between 900 and 600 hPa, while C and D present the V_T in all vertical extension, relating the V_T between 900 and 600 hPa, and between 600 and 300 hPa (parameters $-V_T^L$ and $-V_T^U$). The diagrams provided by FSU have constant intervals for the axes of the diagrams, regardless of the intensity of the cyclone analyzed, which may cause difficulty in interpreting the diagrams of less intense cyclones. To overcome this limitation, figures B and D correspond to the same values of the parameters of the original graphics of figures A and C. However, the scale of the graphics has changed so that there is a greater understanding of the evolution of the cyclone.

In Figure 7 (A and B) it is possible to notice that, between the 14th and the 15th, the cyclone Arani presented strong thermal symmetry (B approximately zero) and warm core between 900 and 600 hPa ($-V_T^L$ around +50), occupying the typical space of subtropical cyclones in the phase diagram. Throughout the 15th, there was a strengthening of the warm core at low levels, coinciding with the increase in its convective activity (Figure 1) and the elevation of the cyclone category from depression to subtropical storm, due to the intensification of winds. During the 16th, there was a reduction in the thermal symmetry of the cyclone and a reduction in the warm core intensity. On the 17th, the diagrams pointed to a transition of the cyclone from warm core to cold core at low levels and an increase in thermal asymmetry, acquiring the characteristics of a weak extratropical cyclone.

Figure 7 (C and D) shows that the cyclone Arani maintained a weak warm core at low levels and a weak cold core at high levels, from its appearance until the moment it underwent extratropical phase transition on the 17th. This corroborates Hart (2003), who states that subtropical cyclones have a weak warm core structure in the lower troposphere, resulting from a lack of sustained convection near the center of the cyclone.

It is important to emphasize that although the Global Forecast System (GFS) results did not present evidence of the transition (Figure 9), the reanalysis with ERA-Interim (ECMWF) data showed it through the phase diagrams (Figure 7). There was a frontal system further south, and when analyzing satellite images and wind fields, there is strong evidence that there was an interaction between the cold air mass that was in the rear of the cold front and cyclone Arani, at the moment the front comes very close to it. The cold air intrusion may have been small to the point of not altering the positive signal of the thermal wind at low levels, which is evident in the vertical cross sections in the Figure 9, where the cyclone maintains the highest values of the geopotential anomalies near the surface. However, there may have been an increase in the asymmetry of the cyclone, which is evident by the phase diagrams (B between 15 and 25 meters) and by the intensification of winds at the time of the probable phase transition, when the potential energy of the cyclone increases due to the increase in asymmetry, having consequently a response in wind intensity.

Elsberry (1995) showed that wind intensity increases significantly during and immediately after the extratropical transition process. This occurs, as perceived by Pálmen (1958), as a result of the increase in the potential energy available in the atmosphere due to the increased asymmetry of the cyclone. In the case of the cyclone Arani, during and after the extratropical transition pointed out by the phase diagrams, from 171200Z (Figure 7), the winds at 10 meters intensified (Figure 8). Considering that on the 16th and the 17th the warm core of the system was weakening and the wind intensity was declining, the new wind inten-

S&G Journal
Volume 15, Number 3, 2020, pp. 235-249
DOI: 10.20985/1980-5160.2020.v15n3.1663

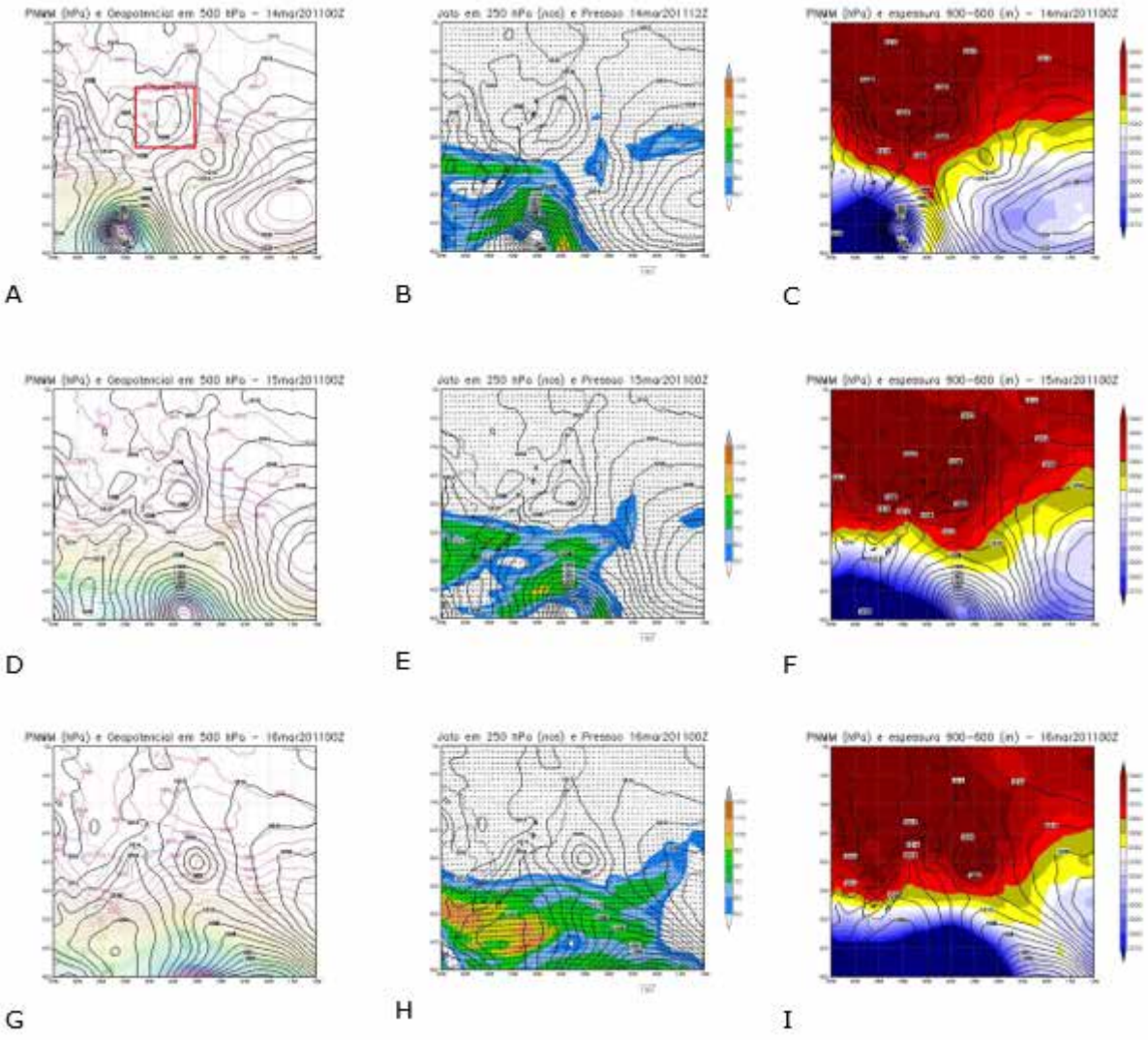

Figure 5. Pressure at Sea Level (contours in black) and: I) geopotential height in 500 hPa (colored contours); II) winds (arrows) and jets in 250 hPa (colored) and III) layer thickness between 900 hPa and 600 hPa (colored), according to CFSR reanalysis.

S&G Journal
Volume 15, Number 3, 2020, pp. 235-249
DOI: 10.20985/1980-5160.2020.v15n3.1663

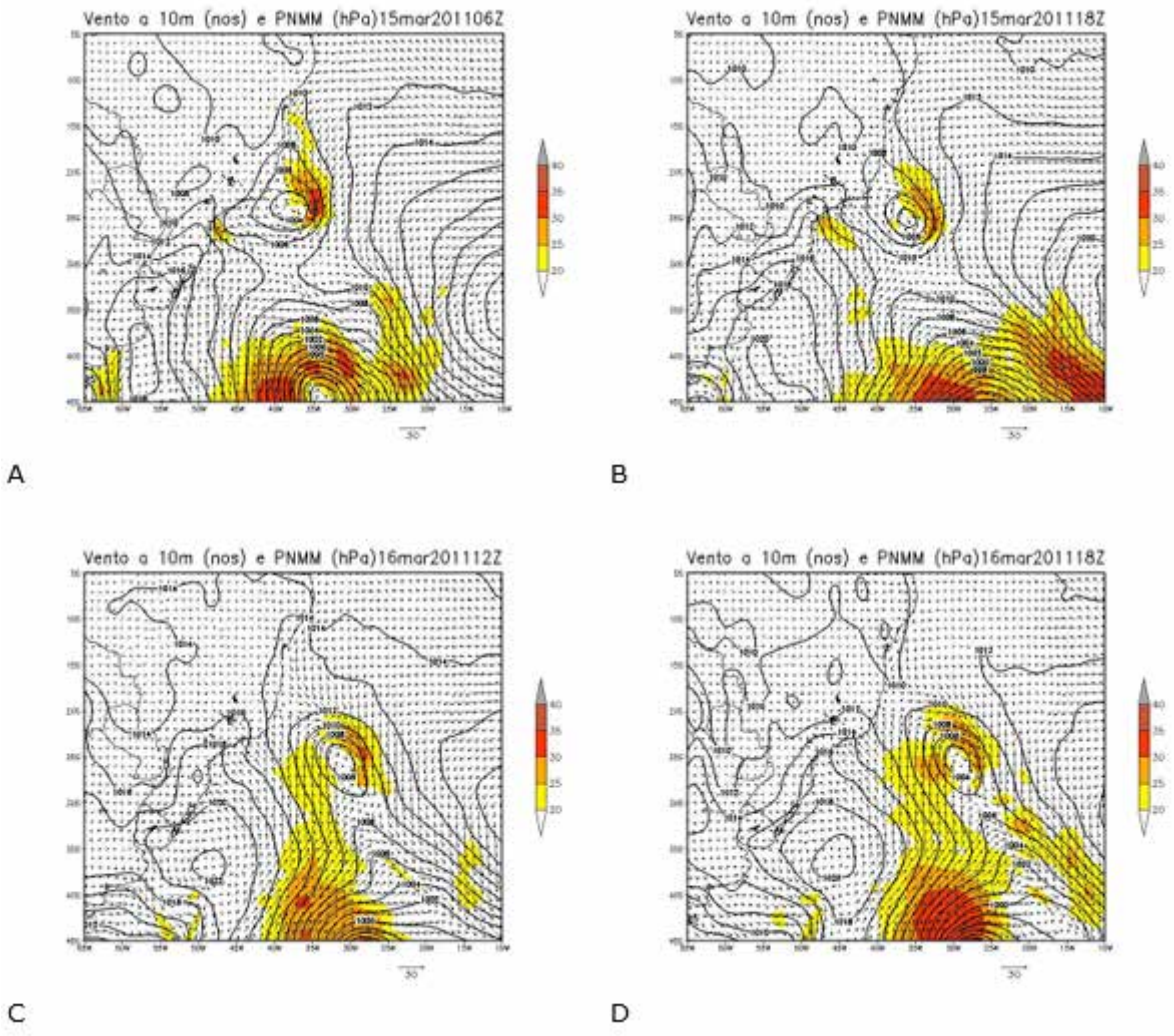

Figure 6. Wind fields at 10 meters from the CFSR reanalysis.

sification in the southwest portion of the cyclone occurred as a consequence of the increase in the potential energy of the system, as indicated by the symmetry parameter of the phase diagram.

The warm core structure acquired by the cyclone Arani can be identified by the vertical cross section of geopotential anomaly (Figure 9). It can be noted that the Arani cyclone had a warm core restricted to the low levels of the troposphere: the largest negative geopotential anomalies were at the base of the cyclone, and the trough axis was practically vertical. According to the reanalysis data, the warm core pattern at low levels and cold core at high levels was maintained throughout its life cycle, which can be verified by the positive values of $-V_T^L$ and negative $-V_T^U$ in the geopotential disturbance profiles. The $-V_T^L$ values decreased with time, showing a tendency of weakening of the warm core; however, there was no change in the signal that should occur in an extratropical transition.

The vertical profiles (Figure 9) do not show the appearance of a cold core at low levels, contrary to the information contained in the phase diagrams. Nevertheless, the possible occurrence of the extratropical transition shown by the phase diagrams is coherent with an interaction of the cyclone Arani with the cold air mass that moved in the rear of the cold front further south, when the two meteorological systems approached on the 17th.

The possibility of the cyclone not having made a complete extratropical transition, only increasing its asymmetry, without changing the thermal wind signal at low levels is not excluded either, as shown by the vertical cross sections of the cyclone's geopotential anomaly. In this case, the Arani would have assumed a hybrid phase at the end of its life cycle, becoming an asymmetric cyclone with a warm core at low levels, and not an extratropical cyclone with a deep cold core and without an associated cold front.

S&G Journal
Volume 15, Number 3, 2020, pp. 235-249
DOI: 10.20985/1980-5160.2020.v15n3.1663

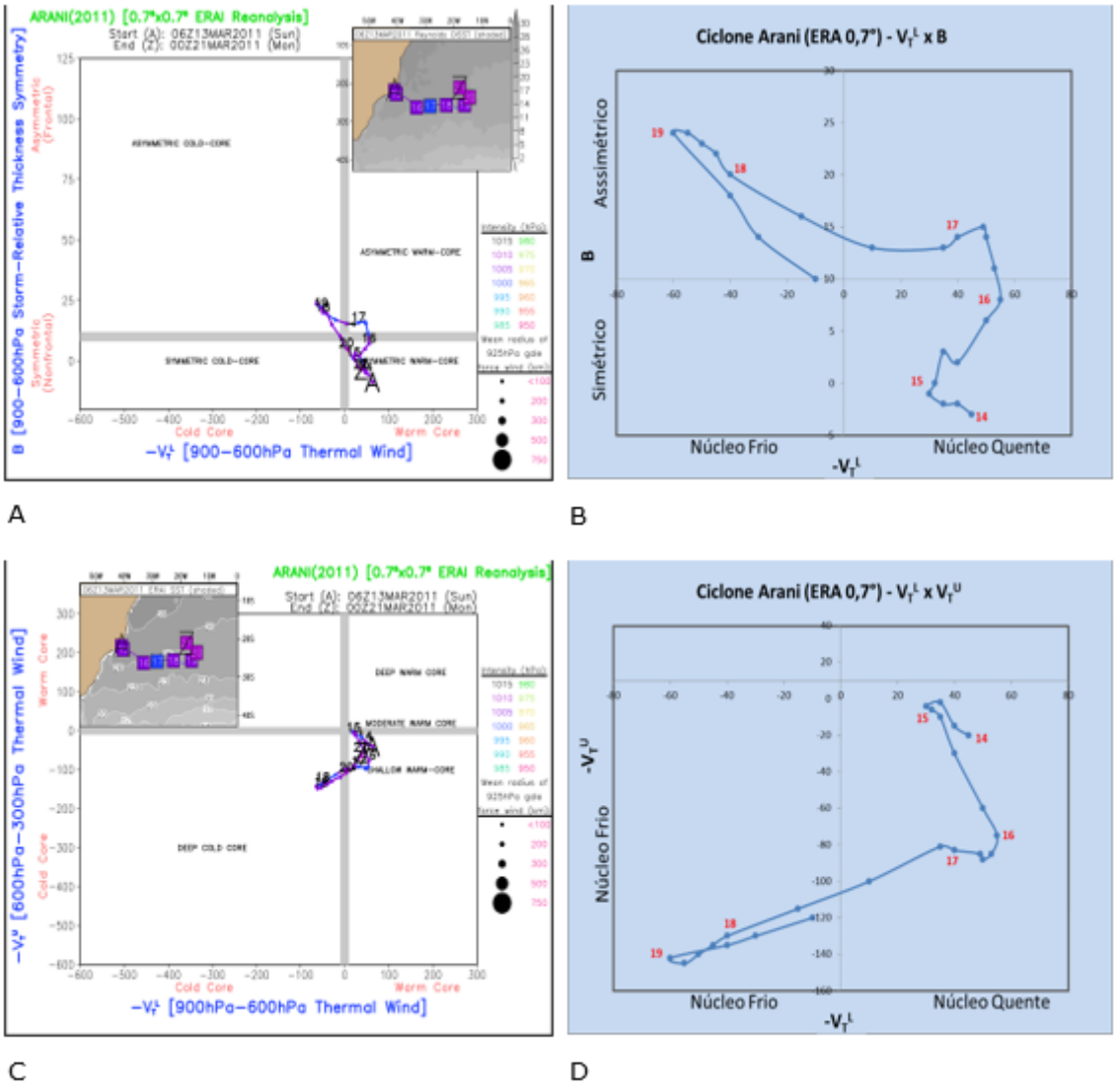

Figure 7. Phase diagrams relating parameters B and $-V_T^L$ (A) and $-V_T^L$ and $-V_T^U$ (C), using the ERA-Interim (0.7) reanalysis. (B) and (D) indicate phase diagrams corresponding to the originals (A and C), with scale change. [Source: A and C Florida State University]

4. CONCLUSIONS

Cyclone Arani was classified as a subtropical cyclone from its origin until the 17th; however, it was a subtropical depression from the 14th until the 15th, when it reached the intensity of the subtropical storm. From the 17th on, the cyclone performed extratropical transition (complete or partial, depending on the data source used - ERA-Interim or CFSR) and remained in that phase until its dissipation. It should be noted that this phase transition may have been partial (only the asymmetry increased, keeping the warm core), which would classify it as hybrid after the subtropical phase, or it may have been total (becoming asymmetric and cold core), according to the results of the diagram.

The cyclone presented subtropical characteristics easily identified in the phase diagrams, contributing to the understanding of its cloud coverage, intensity, and path. According to the diagrams, after its initial intensification, the warm core lost intensity continuously and underwent an extratropical transition when influenced by a frontal system that moved south of the cyclone.

Despite the disagreement of ERA-Interim and CFSR reanalyses, regarding the occurrence of the extratropical phase transition at the end of its life cycle, it is a consensus between the diagrams and the reanalysis data that the cyclone Arani did not perform a complete tropical transition. To reach the category of a tropical storm or hurricane, the

S&G Journal
Volume 15, Number 3, 2020, pp. 235-249
DOI: 10.20985/1980-5160.2020.v15n3.1663

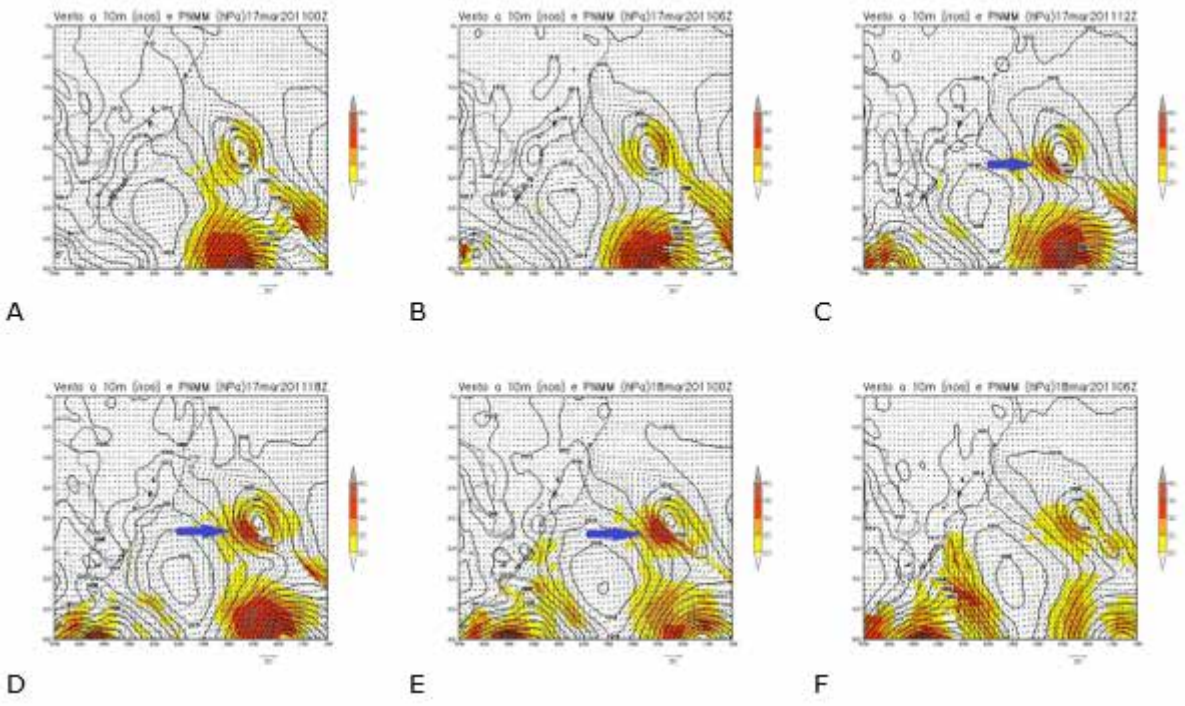

Figure 8. Pressure at Mean Sea Level (PMSL) and wind at 10 meters. The blue arrows highlight the area where the winds intensified.

cyclone should have a deep warm core. Its tropical development was restricted by ambient conditions, such as the vertical wind shear and the approach of a middle latitudes baroclinic wave.

As expected for cases of extratropical transition, there was a further intensification of winds during the period of decline before the phase transition of cyclone Arani. As seen previously, other researchers had already reached a conclusion on the intensification of cyclones with tropical characteristics during and after the extratropical transition, showing that phase diagrams are important tools in predicting changes in cyclone intensity.

To detect structural and thermal variations of cyclones with tropical characteristics and smaller spatial dimensions and intensities, such as the Arani cyclone, it is necessary to use appropriate models and adjust the scale of the diagrams so that they represent well the typical values of these systems, which are usually smaller in module. The phase diagrams of cyclones with weak warm core, obtained from results of global models, should be carefully analyzed and their qualitative study is more important than the quantitative one.

Phase diagrams can be a valuable contribution in forecasting cyclones, especially in the South Atlantic Ocean, where the scarcity of observations does not allow real-time monitoring of their changes in structure and intensity.

ACKNOWLEDGMENTS

To Dr. Robert Hart of the University of Florida, who has always been accessible and willing to help, since the International Meeting on South Atlantic Cyclones, held in Rio de Janeiro in 2008, either by providing the diagrams analyzed in this paper, or by contributing to the analysis of cyclone phase transitions.

REFERENCES

Doty, B.E.; Kinter, J.L. 1995. Geophysical Data Analysis and Visualization using GrADS. Visualization Techniques in Space and Atmospheric Sciences. Washington, D.C. NASA, pp. 209-219.

Elsberry, R. L. 1995. Tropical cyclone motion. Global Perspectives on Tropical Cyclones. Tech. Doc. WMO/TD-693, World Meteorological Organization.

Gan, M. A. 2009. Ciclone Catarina: Análise Sinótica. III Simpósio Internacional de Climatologia, Canela, RS, 18 a 21 de outubro de 2009.

Gozzo, L.F. et al. 2014. Subtropical Cyclones over the Southwestern South Atlantic: Climatological Aspects and Case Study. Journal of Climate 27, 8543–8562. https://doi.org/10.1175/JCLI-D-14-00149.1

Hart, R. E. 2003. A cyclone phase space derived from thermal wind and thermal asymmetry. Monthly Weather

S&G Journal
Volume 15, Number 3, 2020, pp. 235-249
DOI: 10.20985/1980-5160.2020.v15n3.1663

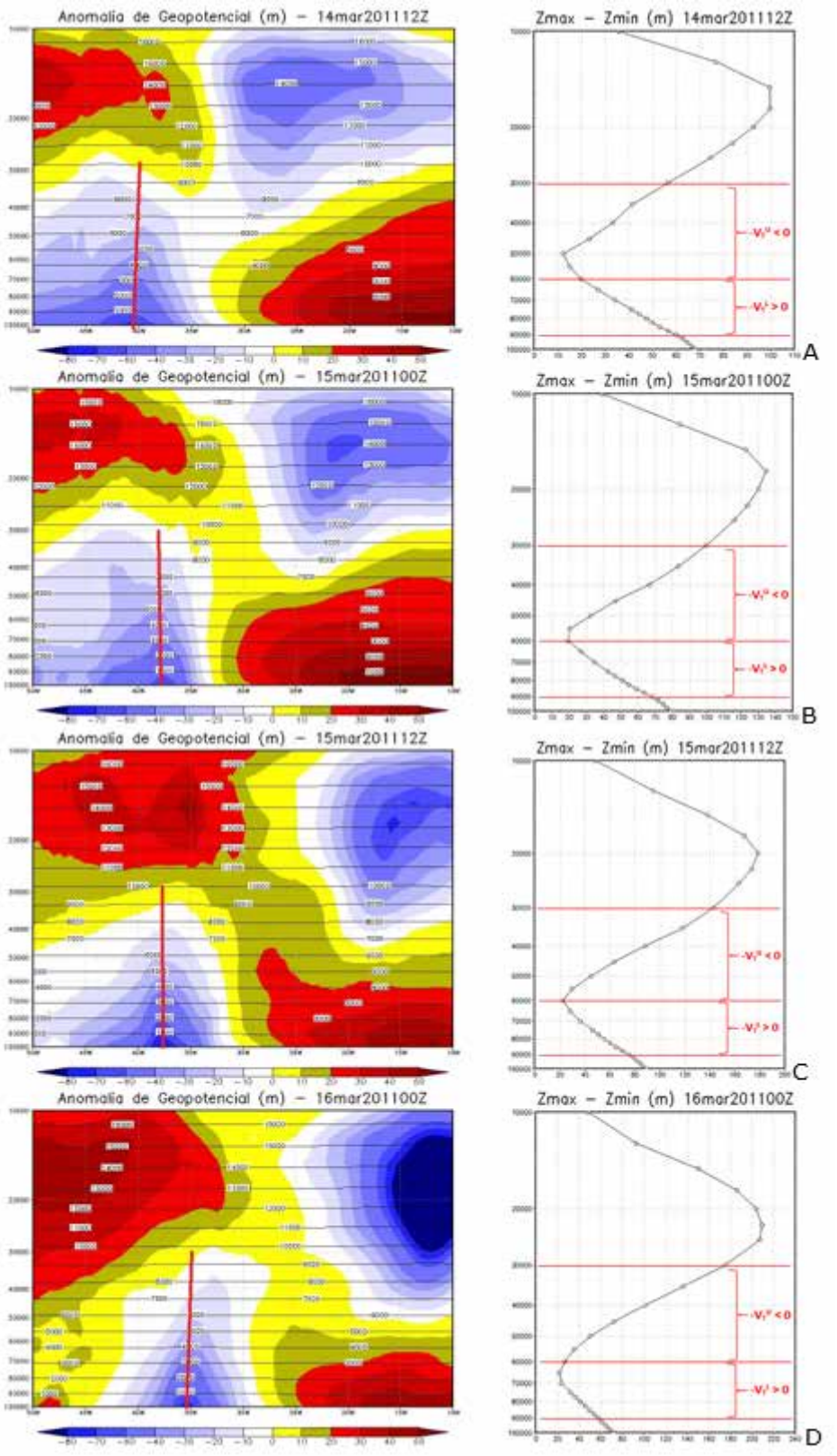

Figure 9. Zonal geopotential anomaly and geopotential disturbance profile (ΔZ = Zmax - Zmin) in a 500 km radius around the cyclone, according to CFSR reanalyses. The axis of the geopotential anomaly and the atmospheric layers used for the cyclone phase analysis (900 hPa - 600 hPa and 600 hPa - 300 hPa) are highlighted in red.

S&G Journal
Volume 15, Number 3, 2020, pp. 235-249
DOI: 10.20985/1980-5160.2020.v15n3.1663

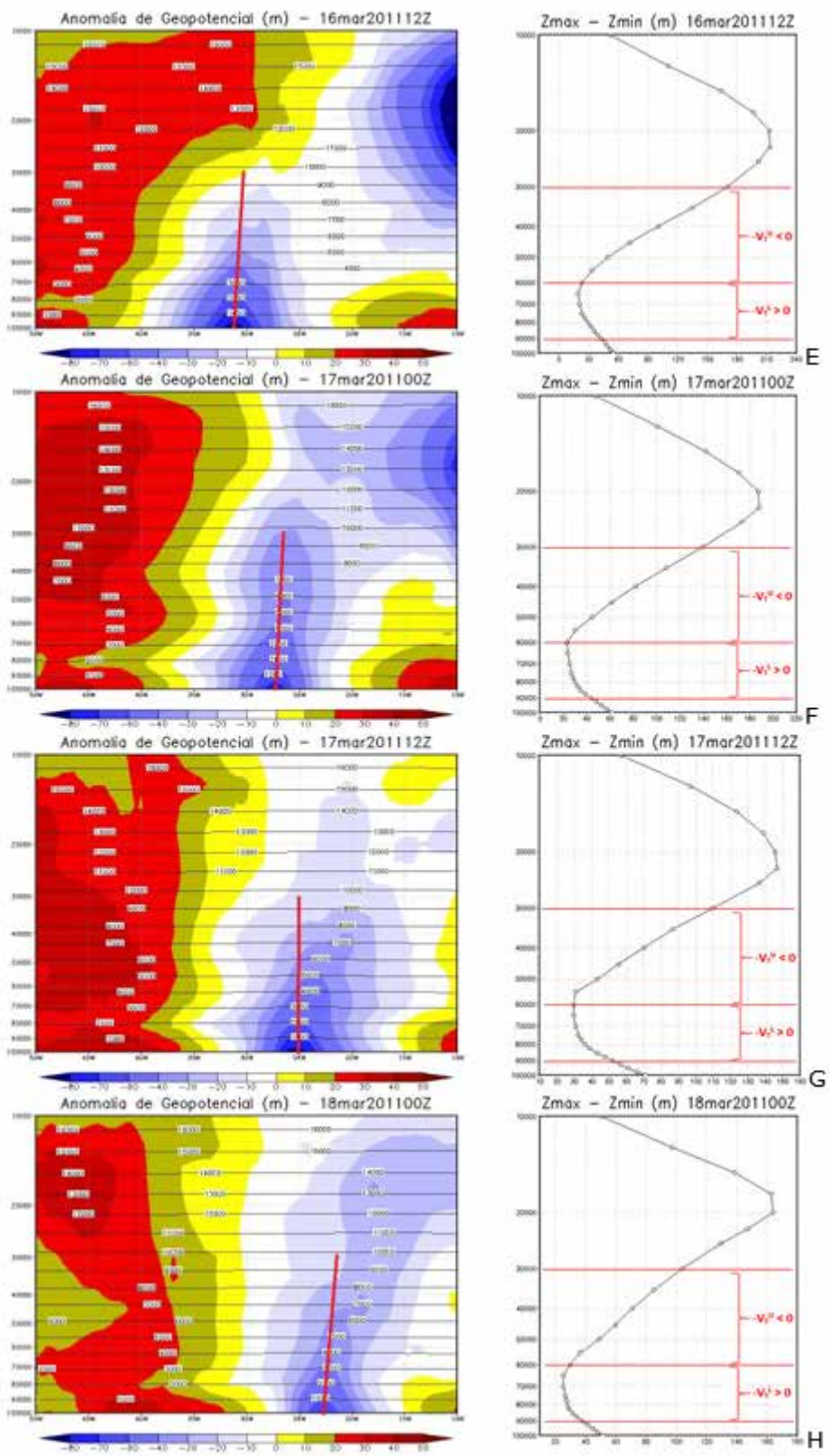

Review 131, 4:585–616. https://doi.org/10.1175/1520--0493(2003)131<0585:ACPSDF>2.0.CO;2

Hart, R. E.; Evans, J. L. A. 2001. Climatology of the Extratropical Transition of Atlantic Tropical Cyclones. Journal of Climate 14, 4:546-564. https://doi.org/10.1175/1520--0442(2001)014<0546:ACOTET>2.0.CO;2

Herbert, P. J.; Poteat, K. O. 1975. A Satellite Classification Technique for Subtropical Cyclones. NOAA tech. Memo. NWS SR-83, National Weather Service.

Hirschberg, P. A.; Fritsch, J. M. 1993. On Understanding Height Tendency. Monthly Weather Review 121, 9:2646–2661. https://doi.org/10.1175/1520-0493(1993)121<2646:OUHT>2.0.CO;2

Jarvinen, B.R. et al. 1984. A Tropical Cyclone Data Type for the North Atlantic Basin, 1886-1983: Contents, Limitations, and Users. NOAA Tech. Memo. NWS NHC 22.

Palmén, E. 1958. Vertical circulation and release of kinetic energy during the development of Hurricane Hazel into an extratropical storm. Tellus 10, 1:1-23. https://doi.org/10.1111/j.2153-3490.1958.tb01982.x

Saha, S. et al. 2010. The NCEP Climate Forecast System Reanalysis. Bulletin of the American Meteorological Society 91, 8:1015–1057. https://doi.org/10.1175/2010BAMS3001.1

Received: 14 Jul 2020

Approved: 02 Nov 2020

DOI: 10.20985/1980-5160.2020.v15n3.1663

How to cite: Palmeira, A.C.; Mathias, R.S.B. (2020). Life cycle study of subtropical cyclone Arani in the South Atlantic in March 2011 through the ERA-Interim and CFSR reanalyses. Revista S&G 15, 3, 235-249. https://revistasg.emnuvens.com.br/sg/article/view/1663